



# Surface Temperature Dependence of Stratospheric Sulfate Aerosol Forcing and Feedback

Ravikiran Hegde<sup>1,2</sup>, Moritz Günther<sup>1</sup>, Hauke Schmidt<sup>1</sup>, and Clarissa Kroll<sup>1,3</sup>

<sup>1</sup>Climate Physics Department, Max Planck Institute for Meteorology, Hamburg, Germany

<sup>2</sup>School of Physics, Indian Institute of Science Education and Research Thiruvananthapuram, Kerala, India

<sup>3</sup>now at: Institute for Atmospheric and Climate Science, ETH Zurich, Zurich, Switzerland

**Correspondence:** Ravikiran Hegde (ravikiran.hegde@mpimet.mpg.de) and Hauke Schmidt (hauke.schmidt@mpimet.mpg.de)

**Abstract.** Stratospheric sulfate aerosol originating from explosive volcanic eruptions can perturb the radiative budget for several years following the eruption. However, the understanding of the state dependence of aerosol forcing and its effect on the radiative feedback is still incomplete. We quantify the contributions to clear-sky forcing and feedback from absorbing and re-emitting longwave radiation, stratospheric heating, and enhanced stratospheric water vapour. We show that, at surface temperatures from 280 K to 300 K, the aerosol forcing becomes less negative (weaker) with increasing surface temperature because its longwave component becomes more positive. Aerosol forcing has a stronger surface temperature dependence than CO<sub>2</sub> forcing. This stronger dependence arises because, unlike CO<sub>2</sub>, the aerosol predominantly absorbs in the spectral range in which the atmosphere is optically thin and thus spectrally masks the surface-temperature dependence of emissions. Additionally, the radiative feedback to surface temperature change is less negative in the presence of the aerosol. This is mainly due to the fact that the temperature of the aerosol layer is largely independent of the surface temperature, leading to a masking of emission changes through the aerosol layer. The study highlights the critical role played by the spectral nature of aerosol longwave absorption in determining the surface temperature dependence of the forcing and in reducing the feedback in comparison to an atmosphere without stratospheric aerosol.

## 1 Introduction

Strong volcanic eruptions can inject sulfur into the stratosphere, where it subsequently forms sulfate aerosol (Hansen et al., 1992; Robock, 2000). By scattering incoming shortwave radiation, the sulfate aerosol increases the planetary albedo, which cools the surface. To a smaller extent, sulfate aerosol also absorbs longwave radiation, which causes a greenhouse effect and partly offsets the cooling.

It has been shown that stratospheric sulfate aerosol forcing causes lower global-mean surface temperature change compared to CO<sub>2</sub> forcing of the same magnitude (Hansen et al., 2005; Boer et al., 2006; Marvel et al., 2016; Gregory et al., 2016; Günther et al., 2022). This disparity was attributed to the stronger feedback to aerosol forcing originating from differences in sea surface temperature response patterns (Günther et al., 2022) and hence tropospheric stability (Salvi et al., 2023). In addition to circulation and pattern effects, purely radiative effects have been found to cause a state dependence of forcing and feedback



to changes in CO<sub>2</sub> levels (Jeevanjee et al., 2021; Stevens and Kluft, 2023). In this work we explore if such a state dependence  
25 of radiative forcing and feedback also exists for stratospheric sulfate aerosol ("aerosol" hereafter), and if purely radiative effects  
may contribute to different feedbacks in atmospheres with and without stratospheric aerosol loading.

Understanding how aerosol forcing depends on the climate state is crucial for analysing the climatic effects of volcanic  
eruptions or the effectiveness of geoengineering attempts in different climate states or at different locations of the Earth. The  
effects of climate change on volcanic aerosol forcing (Aubry et al., 2022) in the light of changes to plume height (Aubry et al.,  
30 2021), anthropogenic pollution (Hopcroft et al., 2017), ocean stratification (Fasullo et al., 2017), and ocean and atmospheric  
circulation (Aubry et al., 2021; Zanchettin et al., 2013) have been studied with contrasting predictions on the change in forcing  
magnitude. However, the purely radiative effects and their dependence on the base state still need to be understood.

Insights on the CO<sub>2</sub> forcing and radiative feedback provide a starting point to understand the state dependence of aerosol  
forcing and the modulation of the feedback. CO<sub>2</sub> forcing originates from the increase in the emission height in the CO<sub>2</sub>  
35 absorption band and can be viewed as a swap of tropospheric or surface emissions with emissions from the stratosphere. Thus,  
the magnitude of CO<sub>2</sub> forcing depends primarily on the temperature contrast of the two layers, and the amount of water vapour  
(Huang et al., 2016; Jeevanjee et al., 2021; Stevens and Kluft, 2023). Drawing parallels to the well-understood CO<sub>2</sub> forcing, the  
aerosol longwave absorption causes a similar greenhouse effect. However, the forcing may show a different state-dependence  
for three reasons. First, climate-relevant volcanic eruptions typically have an aerosol profile that peaks in the stratosphere in  
40 contrast to the well-mixed CO<sub>2</sub>. Second, sulfate aerosol is a broadband absorber, while CO<sub>2</sub> absorbs in a relatively narrow and  
prominent spectral band. Third, stratospheric heating by the aerosol and the increase in water vapour concentration can also  
contribute to the forcing. In this paper we will disentangle and quantify these effects.

The clear-sky longwave radiative feedback has been shown to weaken rapidly between surface temperatures of 280 K and  
300 K (Koll and Cronin, 2018; Kluft et al., 2021; Seeley and Jeevanjee, 2021). The weakening was attributed to the closing  
45 of the atmospheric emission windows, the spectral region where water vapour is optically thin (Kiehl and Trenberth, 1997),  
typically between 750 cm<sup>-1</sup> and 1250 cm<sup>-1</sup>, due to an increase in atmospheric water vapour. The additional presence of  
aerosol, which unlike CO<sub>2</sub> strongly absorbs in the atmospheric window, may mask the surface response further and result in  
weaker radiative feedback.

To summarize, we address the following questions in this work: How much do the individual aerosol radiative effects con-  
50 tribute to the aerosol forcing? How much does the presence of aerosol modulate the feedback? How does this contribution  
change with surface temperature? To answer these questions we use radiative transfer calculations and idealized climate sim-  
ulations with the one-dimensional radiative-convective equilibrium (RCE) model *konrad* (Kluft et al., 2019; Dacie et al.,  
2019). The model's simple formulation, unhindered by complex interactions present in General Circulation Models (GCMs),  
allows us to provide a mechanistic understanding of the clear-sky radiative changes instigated by stratospheric sulfate aerosol  
55 and how they shape the forcing and feedback at climate states with different surface temperatures.



## 2 Methodology

### 2.1 Model setup

The study is performed with `konrad` (Kluft et al., 2019; Dacie et al., 2019), a one-dimensional radiative-convective equilibrium model. We choose this model as it offers a high flexibility to control the atmospheric composition, vertical humidity profiles, surface attributes and lapse rate, allowing us to isolate important processes and provide a mechanistic understanding. `konrad` also makes it possible to run simulations at a high vertical resolution to numerical equilibrium at low computational cost.

`konrad` accounts for convection by adjusting the temperature profile to a moist-adiabatic lapse rate. This convective adjustment results in a distinct convective top. Below the convective top, the atmosphere is in radiative-convective equilibrium, and the surface temperature sets the temperature profile. Above the convective top, the atmosphere is in a radiative equilibrium. We use 512 pressure levels in the atmosphere with a spacing that increases linearly in logarithmic pressure space ranging from 1000 hPa to 0.1 hPa (Kluft et al., 2019). In the troposphere, the relative humidity (RH) is fixed at 80% following Kluft et al. (2021). Above the cold point tropopause (i.e. in the stratosphere), the water vapour volume mixing ratio is set to its value at the cold point. The pattern of surface warming and changes in circulation are not accounted for in the one-dimensional simplification.

`konrad` uses the Rapid Radiative Transfer Model for GCMs (RRTMG, Mlawer et al. (1997) to calculate the radiation. RRTMG has been shown to produce results similar to line-by-line calculations for surface temperatures up to 305 K (Kluft et al., 2019, 2021). Following Wing et al. (2018), the solar constant is set to  $551.58 \text{ W m}^{-2}$  at a zenith angle of  $42.05^\circ$ , resulting in a top of the atmosphere solar insolation of  $409.6 \text{ W m}^{-2}$ , which is equal to the annual mean insolation of the tropics ( $0^\circ$  to  $20^\circ$ ). The surface albedo is set to 0.2 to account for the missing cloud albedo in our clear-sky setup.

The Easy Volcanic Aerosol (EVA) forcing generator (Toohey et al., 2016) is employed to generate a vertical profile of aerosol optical properties (extinction, single scattering albedo, asymmetry parameter) for the RRTMG bands, which is then prescribed in the model. We utilize the aerosol optical profile, representing spatially averaged values between  $23^\circ\text{N}$  and  $23^\circ\text{S}$ , six months after equatorial eruptions with injection masses of 10 Tg and 20 Tg sulfur. We name these cases “Tg10” and “Tg20”, respectively. The largest extinction coefficients are found between 18 km and 25 km altitude, as seen in Fig. 1(a). While forcing due to a realistic volcanic eruption would first increase and then decrease within a time frame of only a few years, we study an idealized abrupt stratospheric sulfate aerosol forcing, which is static. The simplification allows us to examine how the radiative forcing and modulation of the radiative feedback emanating from sulfate aerosol injection in the stratosphere depend on surface temperature.

### 2.2 The forcing-feedback framework

We analyse the aerosol perturbation within the forcing-feedback framework (Gregory et al., 2004; Forster et al., 2021). If a climate state in equilibrium is perturbed, for example, by a change in  $\text{CO}_2$  concentration or introduction of an aerosol layer, this will result in a radiative forcing  $F$  (positive downwards) and an imbalance in the top-of-atmosphere (TOA) net flux  $N$ . To



regain equilibrium (i.e.  $\Delta N = 0$ ), the climate system adapts via a radiative response  $R = \lambda \Delta T_s$  (positive downwards) mediated through a change in surface temperature  $T_s$ . The energy balance of the evolving climate state can be represented by,

$$\Delta N = F + \lambda \Delta T_s. \quad (1)$$

$F$ , also referred to as the effective radiative forcing (Forster et al., 2016), includes rapid *adjustments* such as changes to the stratospheric temperature. The feedback parameter  $\lambda$  (Hansen et al., 1997; Rugenstein and Armour, 2021) quantifies the ability of the system to adjust to the imposed perturbation through a change in surface temperature. A negative  $\lambda$  drives the system to a new equilibrium state, thus representing a stable climate.

An estimate of the change in surface temperature at the new equilibrium  $\Delta T_{eq}$  due to the imposed perturbation can be computed as

$$\Delta T_{eq} = -\frac{F}{\lambda}. \quad (2)$$

### 2.3 Simulations

We consider two types of perturbation of the climate system over a temperature range of 280 K to 300 K: first, a halving of  $\text{CO}_2$  concentrations, and second, the introduction of two different sulfate aerosol loadings formed from sulfur injections of 10 Tg and 20 Tg. For the  $\text{CO}_2$  forcing scenario, the  $\text{CO}_2$  concentration is abruptly changed throughout the atmospheric column, and for the aerosol forcing scenario, the aerosol optical properties are prescribed abruptly.

To calculate the effective forcing, we run `konrad` with a fixed surface temperature and pre-industrial concentrations for greenhouse gases other than  $\text{CO}_2$  until it reaches a radiative-convective equilibrium. A simulation with no aerosol injection and a vertically uniform  $\text{CO}_2$  concentration of 348 ppmv serves as a reference state throughout the study. After perturbing the system, the new equilibrium state is compared to the initial equilibrium to evaluate the effective forcing (Shine et al., 2003; Hansen et al., 2002). For these perturbations, the TOA forcing is given by

$$F = N^p - N^o \quad (3)$$

where  $N^p$  and  $N^o$  are the net TOA fluxes from the perturbed and the reference climate state for the given surface temperature.

To evaluate the feedback parameter, the surface temperature is changed by 2 K, and the system is allowed to equilibrate. The final equilibrium states corresponding to surface temperatures of  $T_1$  and  $T_2 = T_1 + 2\text{K}$  are used to evaluate the feedback parameter at  $(T_1 + T_2)/2$  as (Seeley and Jeevanjee, 2021; Kluft et al., 2021),

$$\lambda = \frac{N_{T_1} - N_{T_2}}{T_1 - T_2}. \quad (4)$$

In Eq. 4, the difference is calculated between the TOA fluxes at two different surface temperatures, either in the presence of the radiative perturbation or in the reference state.

Calculating climate sensitivity using Eq. 2 with  $F$  and  $\lambda$  from fixed surface temperature simulations can yield erroneous values as it does not account for the changes in  $F$  and  $\lambda$  when the system and its surface temperature evolve to a new equilibrium state. Thus, in addition to fixed surface temperature simulations, we perform simulations where the atmospheric column



120 is coupled to a slab ocean with prognostic surface temperature to diagnose the climate sensitivity to aerosol forcing more accurately.

### 3 The aerosol radiative effects

In our analysis of forcing and feedback we will follow the nomenclature by Stevens and Kluft (2023). They define **sensitive emitters** as those whose emission temperature changes with surface temperature. The surface is the most trivial example  
 125 of a sensitive emitter. **Invariant emitters** are emitters whose emission temperature is independent of surface temperature. According to Simpson's law (Simpson, 1928), the tropospheric water vapour at a fixed relative humidity is an example of an invariant emitter. **Spectral masking** happens when invariant emitters mask the response of sensitive emitters.

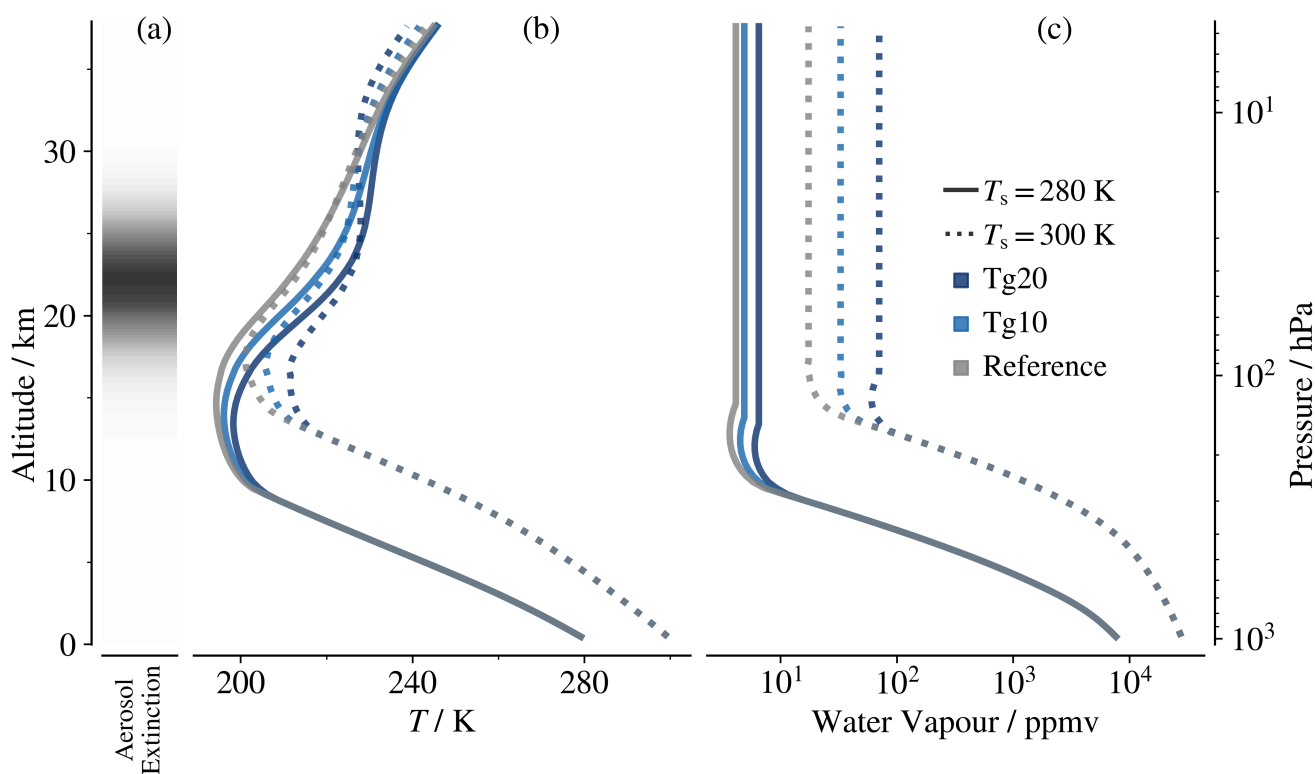


**Figure 1.** The aerosol longwave effects. Vertical profiles of (a) spectrally averaged longwave extinction coefficient in the Tg20 experiment, (b) temperature and (c) water vapour concentration at equilibrium for  $T_s = 280$  K (solid) and  $T_s = 300$  K (dotted). While shades of blue illustrate aerosol injection of different strengths, the grey lines show the reference state. The altitude represented in (a) is calculated from the atmospheric state with  $T_s = 300$  K.

In our study, we elaborate on the three longwave radiative effects of stratospheric aerosol:



130

1. Longwave absorption and re-emission: The longwave absorption by the aerosol layer causes a greenhouse effect. The resulting positive forcing is proportional to the difference in emission temperatures of the surface (or troposphere) and the aerosol layer. The temperature of the stratosphere (and aerosol layer) changes very little with the surface temperature, as seen in Fig. 1(b), making the aerosol an almost invariant emitter. Thus, it partly masks the change in surface emissions with surface temperature.

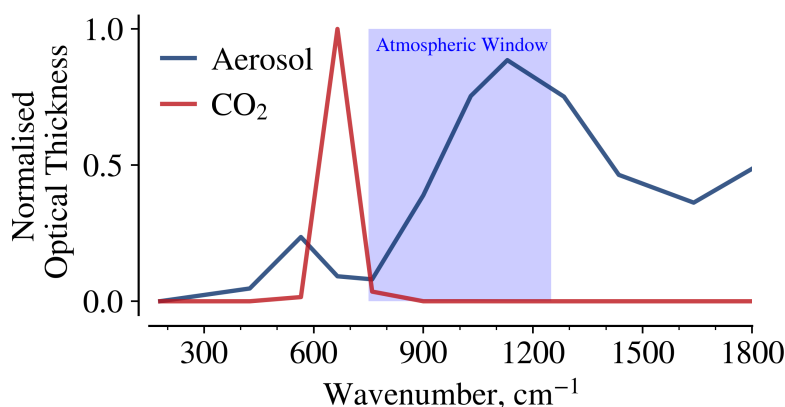


**Figure 2.** Spectral longwave absorption for aerosol and CO<sub>2</sub>. The blue shaded region shows the atmospheric emission window between 750 cm<sup>-1</sup> and 1250 cm<sup>-1</sup> where water vapour is optically thin.

135

2. Stratospheric heating: Introducing a weak absorber in the stratosphere that absorbs in spectral regions where the atmosphere is optically thin results in radiative warming (Shine and Myhre, 2020). Figure 2 shows that the sulfate aerosol absorbs in the spectral range of the optically thin atmospheric window, i.e., where the troposphere emits at high temperatures. Hence, temperatures increase in the lower stratosphere and upper troposphere (Fig. 1b). As a result, the atmosphere emits more longwave radiation at those heights than in the reference state not only because of a higher concentration of the absorber (included in our point 1.) but also because all emitters in that altitude region emit at higher temperature. This effect adds a negative contribution to the TOA radiation balance. Note, that this aerosol effect is unlike the effect of an increase of stratospheric CO<sub>2</sub> which absorbs strongly in a spectral region where the tropospheric emissions originate from relatively low temperatures and, therefore, cools the stratosphere.

140

145

3. Water vapour increase: Due to the fixed relative humidity in the troposphere, the upper tropospheric warming increases the water vapour concentration in the upper troposphere and stratosphere (Joshi and Shine, 2003; Löffler et al., 2016; Kroll et al., 2023), as is also shown in Fig. 1(c). Previous studies have shown that the stratospheric water vapour plays an important role in modulating the rate of global warming (Solomon et al., 2010; Wunderlin et al., 2024). However, it has also been noted in an earlier study (Kroll et al., 2021) that the stratospheric water vapour increase caused by a warmer tropopause reduces the strong negative forcing from stratospheric aerosol only weakly.



Using `konrad` we diagnose the contributions from each aerosol longwave effect individually. For example, the effect of the aerosol's longwave absorption and re-emission alone is determined by the change in the TOA radiative flux caused by introducing the aerosol layer while fixing the temperature and specific humidity profiles from the reference atmospheric state. Similarly, the change in the TOA radiative flux caused by prescribing the changed temperature profile without introducing the aerosol layer or the changed specific humidity profile provides the contribution from the stratospheric warming caused by the aerosol.

In the following sections, we analyse how these three effects come together to produce the differences in the forcing and feedback between aerosol injections and  $\text{CO}_2$  concentration change. We also analyse their dependence on the surface temperature. The aerosol forcing and feedback are calculated from Eq. 3 and Eq. 4, and examined by decomposing them into their longwave and shortwave components.

#### 4 Forcing

Figure 3 shows the surface temperature dependence of the shortwave and longwave components of the forcing due to changes in  $\text{CO}_2$  levels and aerosol. The net  $\text{CO}_2$  forcing arises from the longwave component and is almost independent of temperature between 280 K and 300 K. This behaviour is in agreement with previous studies (Jeevanjee et al., 2021; Kluft et al., 2021). The aerosol forcing is negative in the shortwave and positive in the longwave. The net aerosol forcing (sum of longwave and shortwave components) is negative due to the stronger negative forcing in the shortwave bands. However, it becomes less negative with temperature increase, as the positive longwave component has a more pronounced temperature dependence. Between 280 K and 300 K, the Tg20 aerosol forcing changes approximately from  $-9 \text{ W m}^{-2}$  to  $-6 \text{ W m}^{-2}$  (34%), and the Tg10 aerosol forcing changes from  $-5 \text{ W m}^{-2}$  to  $-4 \text{ W m}^{-2}$  (20%). The  $0.5 \times \text{CO}_2$  forcing changes only by 3% in the same temperature range. The aerosol forcing shows a stronger temperature dependence than the forcing due to a change in  $\text{CO}_2$  levels.

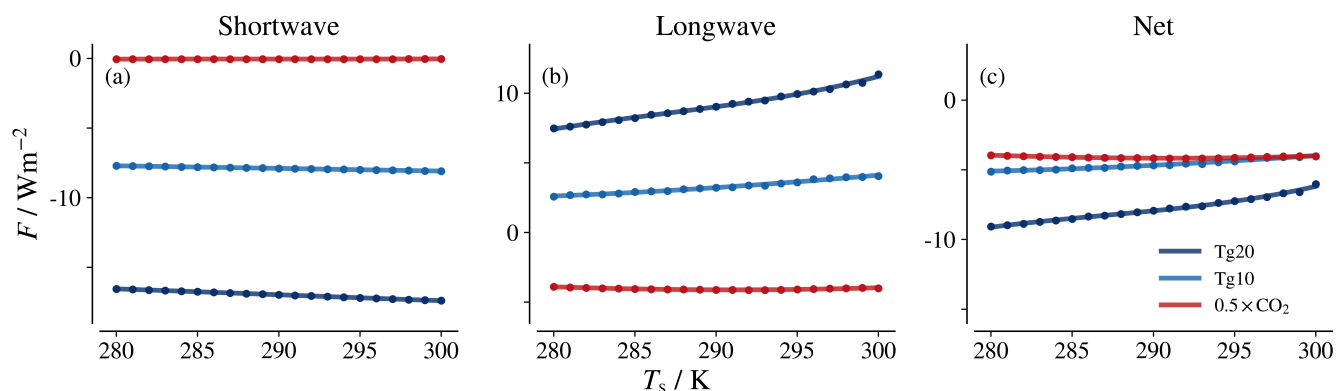


**Figure 3.** Surface temperature dependence of  $\text{CO}_2$  and aerosol forcing  $F$  decomposed into shortwave and longwave contributions as well as the total net forcing. Cubic fits for each set are plotted as solid lines.



## 170 4.1 Forcing in the shortwave bands

As shown in Fig. 3(a) the shortwave aerosol forcing becomes slightly more negative at higher surface temperature. This can be explained by the fixed relative humidity which leads to an increased amount of water vapour in the atmosphere at higher surface temperatures. Introducing a reflective aerosol layer atop of a more absorbing background results in a more negative forcing, because reflection makes a bigger difference over a darker background. The water vapour increase due to the tropopause warming by the aerosol layer is also larger at higher surface temperatures as shown in Fig. 1(c), which further increases the atmospheric absorption.

## 4.2 Forcing in the longwave bands

The longwave component of the aerosol forcing ( $F^{LW}$ ) becomes more positive with increasing surface temperature. This arises due to an interplay of the different aerosol effects on longwave radiation described in Section 3. Below, we analyse the individual contributions of these effects decomposed using radiative transfer calculations. The corresponding results are summarized in Table 1.

Case	$T_s$ (K)	$F^{LW}$	$F_{abs} + F_{\delta T} + F_{\delta q}$	Residual	$F_{abs}$	$F_{\delta T}$	$F_{\delta q}$
Tg10	280	2.66	2.98	-0.32	4.22	-1.36	0.12
	290	3.29	3.66	-0.37	4.93	-1.45	0.17
	300	4.13	4.47	-0.34	5.31	-1.11	0.26
Tg20	280	7.67	9.35	-1.68	11.71	-2.69	0.32
	290	9.3	11.28	-1.98	13.67	-2.88	0.49
	300	11.55	13.41	-1.86	14.75	-2.22	0.88

**Table 1.** The components of longwave aerosol forcing  $F^{LW}$  from radiative transfer calculations. The values of forcing are in units of  $W m^{-2}$ .

Firstly, aerosol can absorb and emit longwave radiation. Hence, introducing an aerosol layer results in an increase of outgoing longwave radiation emanating from atmospheric levels with much lower temperatures than the surface. This reduces the total outgoing longwave radiation and results in a positive forcing. We call this component  $F_{abs}$ . It represents the instantaneous forcing caused by the aerosol, i.e. the direct radiative effect in the absence of adjustments. The stratospheric heating and subsequent moistening, which we describe in the following, are stratospheric adjustments. Together, the instantaneous forcing and the adjustments constitute the effective forcing.

Secondly, warming the aerosol layer leads to more longwave emission from other atmospheric species at these heights, resulting in a negative forcing  $F_{\delta T}$  relative to the reference state. As shown in Table 1,  $F_{\delta T}$  has a weak and non-monotonous temperature dependence from the interplay between two effects. First, the radiation from the surface and lower atmospheric levels that the aerosol can absorb increases with surface temperature, resulting in more radiative heating. Additionally, at higher surface temperatures, the aerosol layer warming is limited to a smaller region due to the expansion of the tropopause, thus making the radiative heating less effective.





195 Thirdly, the additional water vapour (i.e., change in specific humidity  $q$ ) due to the upper tropospheric warming results in a positive forcing  $F_{\delta q}$ . The magnitude of  $F_{\delta q}$  is much smaller than  $F_{\text{abs}}$  and  $F_{\delta T}$ , but increases at higher surface temperatures.

The residual ( $F^{\text{LW}} - (F_{\text{abs}} + F_{\delta T} + F_{\delta q})$ ) is negative; it corresponds to the additional emission from the aerosol heated by its own absorption.

200 The major contribution to the longwave forcing and its temperature dependence comes from the longwave absorption and re-emission term  $F_{\text{abs}}$ . Although  $\text{CO}_2$  forcing mainly originates from a similar effect, the effect depends strongly on the surface temperature for aerosol, but not for  $\text{CO}_2$ . It is worthwhile to analyse this component further to understand the different surface temperature dependencies.

205 In the atmospheric window ( $750 \text{ cm}^{-1}$  to  $1250 \text{ cm}^{-1}$ ) where the atmosphere is optically thin, the longwave radiation at the TOA emanates mainly from the surface which is a sensitive emitter. Outside the window, the surface emissions are replaced with RH-dependent atmospheric emissions from water vapour. Water vapour is an invariant emitter as its emission temperature remains fixed and uncoupled to the temperature of the surface (Simpson, 1928). A longwave absorber such as  $\text{CO}_2$  or aerosol replaces the surface/atmospheric emissions in their spectral range with emissions from the colder stratosphere, thus the forcing magnitude strongly depends on the temperature contrast of the two emission layers (Huang et al., 2016; Jeevanjee et al., 2021).

210 Line-by-line calculations indicate that the  $\text{CO}_2$  forcing originates primarily from the band between  $550 \text{ cm}^{-1}$  and  $800 \text{ cm}^{-1}$  (Pierrehumbert, 2011; Wilson and Gea-Banacloche, 2012; Kluft et al., 2021; Jeevanjee et al., 2021; Stevens and Kluft, 2023) (see also Fig. 2). In the surface temperature range of our study, the forcing primarily emanates from the band center, whose emissions occur at stratospheric heights and are invariant with surface temperature. As this band lies outside and at the edge of the atmospheric emission window, the invariant emitter  $\text{CO}_2$  absorbs and re-emits the emissions from the tropospheric water vapour which is also an invariant emitter. Thus, the fixed emission temperature of the water vapour outside the atmospheric window and the fixed emission temperature of the  $\text{CO}_2$  band center in the stratosphere results in an almost unvarying temperature contrast between the two. Hence, the  $\text{CO}_2$  forcing magnitude does not vary much between 280 K and 300 K surface temperatures.

220 While the aerosol layer mainly resides in the lower stratosphere whose temperature is also  $T_s$ -invariant, a significant contribution to the aerosol optical depth comes from within the atmospheric window (Fig. 2). Thus, the aerosol longwave forcing is primarily due to the replacement of emissions from the surface (sensitive emitter) by the emissions from the aerosol layer (invariant emitter). Hence, with an increase in surface temperature, the temperature contrast between the aerosol layer and surface increases and is responsible for the increasing magnitude of  $F_{\text{abs}}$ .

To summarize, the fact that aerosol forcing exhibits a pronounced surface temperature dependence while  $\text{CO}_2$  forcing does not, arises from the different spectral regions in which they absorb.

## 5 Feedback

225 The flux change brought by a mere introduction of the perturbation is captured in the forcing. On the other hand, the feedback parameter  $\lambda$  represents how the climate response changes with surface temperature. We examine how the three longwave

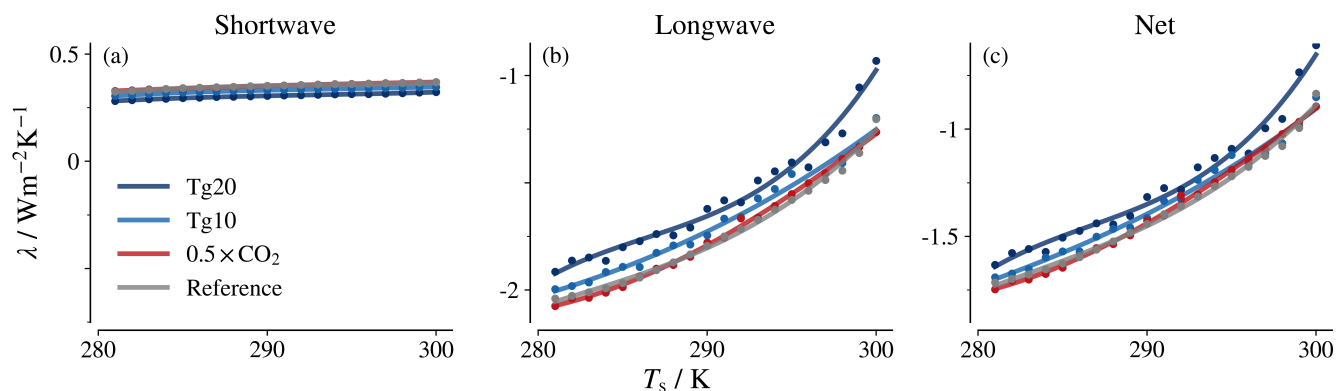


**Figure 4.** Temperature dependence of the feedback parameter  $\lambda$  decomposed into shortwave and longwave contributions. Cubic fits for each set are plotted as solid lines.

effects (longwave absorption and re-emission, temperature change, and water vapour increase) highlighted in Section 3 shape the feedback parameter in the presence of aerosol. The net feedback parameter calculated using Eq. 4 along with the shortwave and longwave components is shown in Fig. 4.

### 230 5.1 Feedback in the shortwave bands

The shortwave component of  $\lambda$  is positive and stems from the absorption of shortwave radiation by the water vapour. It becomes slightly more positive at higher surface temperatures. This can be attributed to the exponential increase in the water vapour amount following the Clausius-Clapeyron relationship at fixed relative humidity. However, the net feedback is dominated by the longwave component, both in absolute terms and with respect to the surface temperature dependence. Changes in surface  
 235 albedo and clouds are not taken into account in our simulations.

### 5.2 Feedback in the longwave bands

The longwave component of  $\lambda$  is negative and depicts the ability of the system to equilibrate by counteracting the energy imbalance through a temperature change of the surface and the surface-coupled troposphere.

The decrease in the magnitude of the longwave feedback parameter between 280 K and 300 K was elucidated using line-  
 240 by-line radiation calculations in Seeley and Jeevanjee (2021); Kluft et al. (2021). They showed that as the surface temperature increases, the atmosphere becomes progressively opaque due to the higher amount of water vapour, and the atmospheric window narrows spectrally, resulting in more of the longwave emission to space emanating from higher up in the troposphere (i.e., lower emission temperatures). This reduces the capability of the system to maintain an energy balance through a change in surface temperature in response to the forcing, which transpires as a weaker negative feedback with an increase in surface  
 245 temperature. Consistent with this explanation, Fig. 4(b) also shows that the temperature dependence of the longwave feedback



for different atmospheric states, defined by different CO<sub>2</sub> concentrations and aerosol loading, is similar to that of the reference state, as the increase in the water vapour amount with surface temperature is ubiquitous.

It can be seen that the feedback parameter does not change much with changes to CO<sub>2</sub> levels from reference to 0.5 × CO<sub>2</sub>. However, in the presence of aerosol the longwave feedback (and thus, the net feedback) becomes weaker with an increase  
250 in the aerosol loading. This is consistent with the temperature dependence of the forcing presented in Fig. 3. Bloch-Johnson et al. (2021) point out that the temperature dependence of CO<sub>2</sub> forcing is equivalent to the CO<sub>2</sub> dependence of the feedback. This is true not only for CO<sub>2</sub> but also for other forcing agents, and hence also aerosol. The positive slope of the temperature dependence of the longwave and total aerosol forcings in Fig. 3 c) and d) requires that the respective feedbacks in Fig. 4 c) and d) are less negative for higher aerosol loading. However, this dependence of the feedback on the aerosol loading is in contrast to  
255 results from GCMs (Günther et al., 2022) where a pattern effect dominates the purely radiative effects. We identify the source of the weaker feedback in the presence of aerosol using radiative transfer calculations.

The feedback calculated in the presence of aerosol forcing  $\lambda^p$  can be expressed as the feedback in the reference state  $\lambda^o$  modulated by the changes introduced due to aerosol  $\Delta\lambda$ :

$$\lambda^p = \lambda^o + \Delta\lambda. \quad (5)$$

260 The net change in feedback due to aerosol  $\Delta\lambda$  is up to first order the sum of the changes due to each of the effects listed in Section 3. That is,

$$\Delta\lambda = \Delta\lambda_{\text{abs}} + \Delta\lambda_{\delta T} + \Delta\lambda_{\delta q} \quad (6)$$

$\Delta\lambda_{\text{abs}}$  represents the direct effect of the longwave absorption and re-emission by the aerosol layer,  $\Delta\lambda_{\delta T}$  represents the effect due to the warming by the aerosol layer, and  $\Delta\lambda_{\delta q}$  represents the effect of specific humidity change. They are calculated as  
265 the difference with respect to the reference state in the longwave component of  $\lambda$ , calculated by radiative transfer calculations with only the associated change present. That is,

$$\Delta\lambda_i = \lambda^{o,i} - \lambda^o. \quad (7)$$

For example,  $\lambda^{o,\text{abs}}$  is the longwave feedback parameter in the presence of the aerosol layer but with the temperature and specific humidity profile of the reference state (i.e. no stratospheric heating or water vapour increase). Analogously,  $\lambda^{o,\delta T}$  ( $\lambda^{o,\delta q}$ )  
270 is the feedback parameter calculated with only the modified temperature profile (specific humidity profile) introduced to the reference state.

The feedback in the Tg20 case is around 0.15 W m<sup>-2</sup> K<sup>-1</sup> more positive (weaker) than the reference across the temperature range, i.e. such an amount of aerosol reduces the net feedback by about 10 – 20 %. While the difference remains relatively constant under surface temperature change, the contribution from the different effects of the aerosol changes. At low temperatures,  
275 the aerosol absorption and re-emission effect dominates, at higher temperatures the contribution from stratospheric warming becomes the leading term (see green and yellow lines in Fig. 5).

The positive (weakening) longwave absorption effect from the aerosol on the feedback ( $\Delta\lambda_{\text{abs}}$ ) originates from spectral masking, and is more effective at lower surface temperatures. The spectral regions in which the aerosol absorbs cannot con-

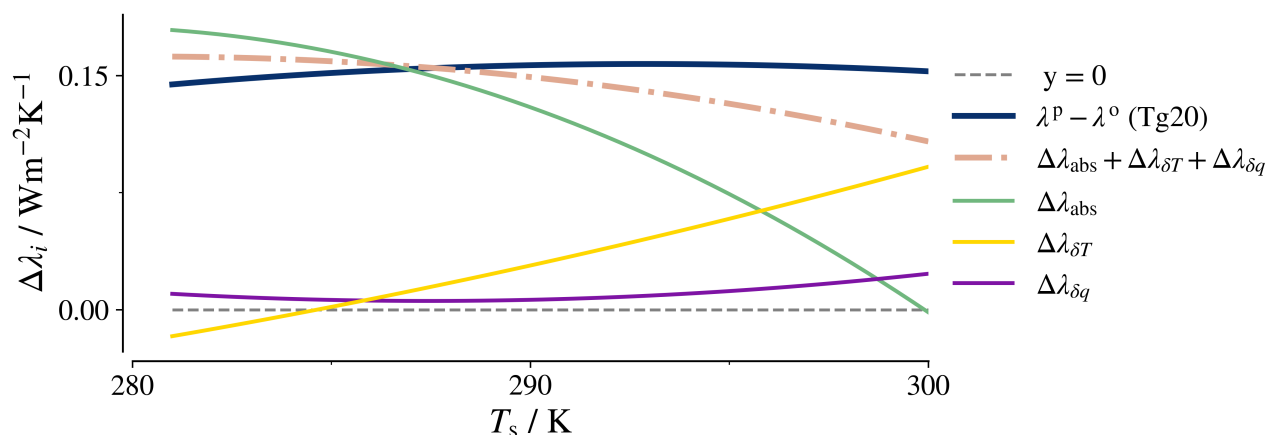


**Figure 5.** The components of modulation of longwave feedback by aerosol from radiative transfer calculations for the Tg20 case. Only the cubic fits through the data points are shown.

tribute to the feedback because aerosol is an invariant emitter, decreasing Earth’s capability to increase outgoing longwave radiation with temperature. As emissions from the surface (sensitive emitter) are replaced by emissions from water vapor (invariant emitter) at higher temperatures due to the closing of the atmospheric window, the spectral masking effect of the aerosol decreases.

The stratospheric warming ( $\Delta\lambda_{\delta T}$ ) contributes positively to the feedback, especially at higher surface temperatures. This effect is in parts artificial and originates from the fact that the height of the aerosol layer is fixed in konrad. With higher surface temperatures, the tropopause shifts upward, which results in the aerosol heating more strongly affecting tropospheric levels. The upper troposphere subsequently does not contribute to the feedback, because its temperature is not set anymore by the surface temperature, but instead by the aerosol heating. This is a positive contribution to the net feedback. However, Aubry et al. (2021) argue that the injection height of volcanic eruptions of the magnitude we study would increase in a warmer climate so that the aerosol layer would remain in approximately the same distance to the tropopause. Even if injection heights would not increase, it is an unrealistic assumption that an aerosol layer could be sustained well below the tropopause. Therefore, the  $\Delta\lambda_{\delta T}$  contribution is somewhat artificial, and we expect that in reality the difference between feedback to aerosol and CO<sub>2</sub> forcing is less pronounced at higher temperatures.

Changes in specific humidity have little influence on  $\lambda$ . Additionally, there is a small residual from the non-linear terms that we neglected in our linear decomposition (difference between yellow dash-dotted and blue line in Fig. 5).

To summarize, the 10 – 20 % weaker radiative feedback in the presence of aerosol is mostly due to the masking effect of surface emissions, which dominates at lower temperatures, and the stratospheric heating, which dominates at higher temperatures.



## 6 Implications for climate sensitivity

Having analysed the forcing and feedback at different surface temperatures, we investigate how their combination, i.e., the surface temperature change at equilibrium as provided by Eq. 2 varies with surface temperature. As the surface temperature change is large (e.g for Tg20,  $\Delta T_{\text{eq}} \approx 6\text{K}$  at  $T_s = 300\text{K}$ ), one has to also account for the change in forcing and feedback magnitudes as the surface temperature evolves. Using the values of  $F$  and  $\lambda$  calculated from fixed-SST simulations would lead to erroneous values of surface temperature change. Simulations with a coupled slab ocean surface with a variable surface temperature incorporate the changes in  $F$  and  $\lambda$ . We determine forcing, feedback, and equilibrium temperature change as  $N$ -intercept, slope, and  $T$ -intercept of  $N(T)$  (Gregory method, Gregory et al. (2004)). This method gives a representative average of the forcing and feedback in the temperature range. Thus, minor differences in the values of  $F$  and  $\lambda$  may be expected when comparing to results from fixed-SST simulations.

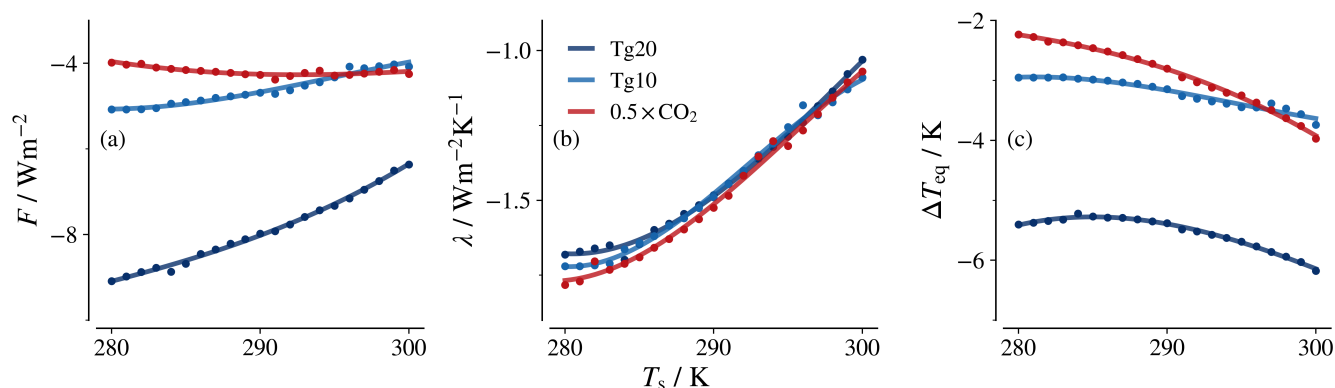


**Figure 6.** Temperature dependence of  $F$ ,  $\lambda$ , and  $\Delta T_{\text{eq}}$  derived from the Gregory method using slab ocean simulations. The x-axis represents the surface temperature at the time of introducing the perturbation. Cubic fits for each set are plotted as solid lines.

Figure 6 shows  $F$ ,  $\lambda$  and  $\Delta T_{\text{eq}}$  calculated from the Gregory method. The forcing and feedback parameter show similar qualitative behaviors when compared to the values obtained from the fixed-SST simulations (Figures 3(c) and 4(c)). The feedback parameters for the different cases become almost indistinguishable at higher surface temperatures. The temperature change in equilibrium shows a weaker surface temperature dependence for aerosol forcing than  $\text{CO}_2$  forcing, because the decrease in absolute value of the forcing at higher surface temperatures partly compensates for the weakening of the feedback parameter. For the Tg20 case, the decrease in absolute values of the forcing with temperature initially dominates over the weakening of the feedback, resulting in a decrease in absolute  $\Delta T_{\text{eq}}$  at lower surface temperatures.

## 7 Dependence on climate state

In the previous sections we studied how the forcing, feedback and climate sensitivity behave for aerosol injections at different surface temperatures, and pointed out the differences to forcing from  $\text{CO}_2$ . However, it is worth noting that the different surface



temperatures studied up to this point are artificial as they do not have a physical driver, but are prescribed to the model. This leads to configurations where e.g. the CO<sub>2</sub> concentration is physically inconsistent with the surface temperature. To generalise the understanding from surface temperature dependence to climate state dependence, we follow the strategy to adjust CO<sub>2</sub> concentrations to the surface temperatures put forward in Romps (2020). We analyse how the forcing and feedback would behave at different surface temperatures driven by a change in CO<sub>2</sub> concentration.

For a fixed surface temperature, the CO<sub>2</sub> concentration is adjusted to reach a closed TOA radiation budget. This represents a CO<sub>2</sub>-induced warming, thus allowing us to analyse the forcing-feedback dependence on the representative climate state. The aerosol injections, or the 0.5 × CO<sub>2</sub> perturbation, are performed relative to these reference states to diagnose the forcing and feedback due to each perturbation.

The CO<sub>2</sub> concentrations at equilibrium at different surface temperatures are shown in Fig. 7(a). It is worth noting that the resultant concentration of CO<sub>2</sub> at low surface temperatures is unrealistic compared to the CO<sub>2</sub> concentrations on Earth. The  $F$  and  $\lambda$  calculated from these simulations, shown in Fig. 7(b) and (c) can be compared to Figures 3(c) and 4(c) when trying to understand which difference comes from the CO<sub>2</sub> concentration.

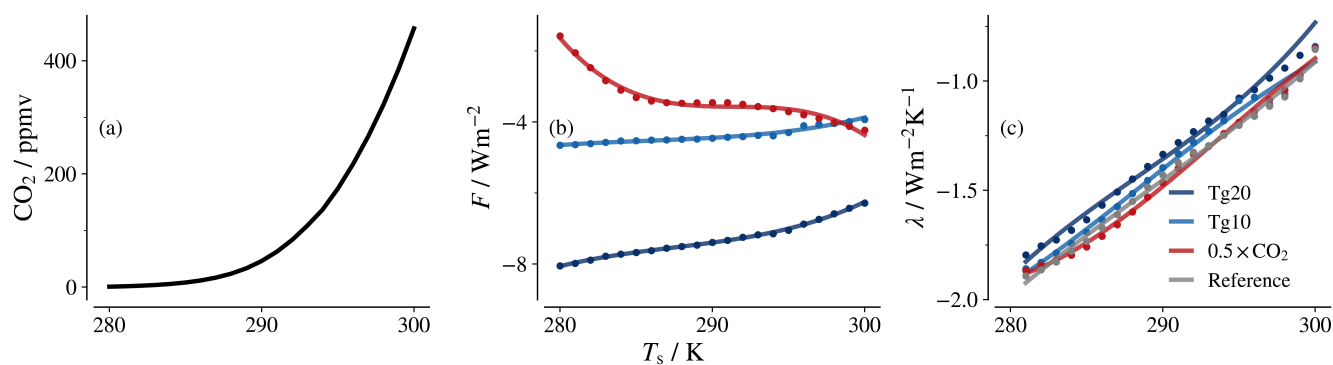


**Figure 7.** Temperature dependence of the CO<sub>2</sub> concentration,  $F$ , and  $\lambda$  in interactive CO<sub>2</sub> simulations. Cubic fits for each set are plotted as solid lines.

Figure 7(b) shows that the 0.5 × CO<sub>2</sub> forcing is weaker for lower temperatures than what is seen in Fig. 3(c). This is due to the significantly lower amount of CO<sub>2</sub> at these temperatures (He et al., 2023). At higher temperatures, the 0.5 × CO<sub>2</sub> forcing shows similar behaviour as depicted in Fig. 3(c) and Fig. 6(a). While slightly weaker in magnitude, the aerosol forcing shows the same qualitative behaviour as noted in earlier sections.

The feedback parameter shown in Fig. 7(c) shows a rapid weakening with increasing surface temperature, similar to that of Fig. 4(c), and as noted in earlier studies (Kluft et al., 2021; Seeley and Jeevanjee, 2021). The weakening of the feedback parameter in the presence of aerosol is also clearly visible.

Thus, the surface temperature dependence we find for forcing and feedback is also valid as a more general climate state dependence. This can be expected as CO<sub>2</sub> and aerosol act on different spectral regions with minimal overlap. The fact that



340 our results do not change substantially even under the unrealistically low background CO<sub>2</sub> concentrations at cold temperatures  
seen in Fig. 7 (a) corroborates that there is little interaction between aerosol and CO<sub>2</sub>.

## 8 Summary and conclusions

We use the 1D-RCE model `konrad` and radiative transfer calculations to provide a mechanistic understanding of the clear-  
sky radiative forcing and feedback mechanisms due to the introduction of aerosol in the stratosphere. Comparing the aerosol  
345 injections to well-studied CO<sub>2</sub> level perturbations, we analyze to which extent the differences can be attributed to three effects  
caused by the aerosol layer, i.e., 1) longwave absorption and re-emission, 2) stratospheric heating, and 3) water vapour increase.  
Among the three effects, longwave absorption and re-emission by the aerosol primarily determines the magnitude and state  
dependence of the longwave aerosol forcing and modulates the radiative feedback. Stratospheric heating weakens the longwave  
aerosol forcing but does not alter the state dependence. The water vapor increase has a negligible impact on both forcing and  
350 feedback.

We show that the net forcing due to aerosol injection has a stronger temperature dependence than forcing due to changing  
CO<sub>2</sub> levels. While the scattering of shortwave radiation results in a negative forcing, the longwave absorption and re-emission  
from the aerosol layer produces a smaller, but more strongly temperature-dependent positive forcing. The longwave forcing  
increases with temperature because stratospheric temperatures are not closely linked to surface temperatures, so that the aerosol  
355 spectrally masks larger emissions resulting from larger surface temperatures. The temperature dependence of longwave forcing  
is far more pronounced for aerosol than for CO<sub>2</sub>, because aerosol unlike CO<sub>2</sub> absorbs in the atmospheric window. Outside  
the window emissions mainly come from water vapour which already masks surface temperature changes. A larger aerosol  
injection would be required at higher surface temperatures to obtain the same forcing magnitude.

We also show that the clear sky radiative feedback in the presence of aerosol follows a similar surface temperature depen-  
360 dence as the reference state or a state with changed CO<sub>2</sub> level. However, the longwave component is consistently weaker at  
all temperatures than that of the CO<sub>2</sub> level perturbations by  $\approx 0.15 \text{ Wm}^2\text{K}^{-1}$  ( $\approx 10 - 20 \%$ ), and thus depends on the nature  
of the forcing. At relatively low surface temperatures, the weaker feedback is dominated by the masking of emissions from  
a sensitive emitter (dominantly the surface) by emissions from a largely invariant emitter, the aerosol layer. At higher surface  
temperatures, the aerosol heating more strongly affects the tropopause layer due to the higher tropopause, which leads to larger  
365 parts of the troposphere being independent of the surface temperature. This constitutes a positive feedback contribution which  
we expect to be largely an artifact of our model setup, because in warmer climates the injection height is projected to increase  
with tropopause height (Aubry et al., 2021) while it is kept fix in our simulations. Furthermore, according to GCM studies the  
Brewer-Dobson circulation would accelerate, which would reduce the warming of the tropical stratosphere (Pitari and Rizi,  
1993; Garcia et al., 2011; Aquila et al., 2013) and influence its emissions.

370 As Bloch-Johnson et al. (2021) point out for the case of CO<sub>2</sub>, also the temperature dependence of the forcing of stratospheric  
aerosol is equivalent to the dependence of the feedback on the aerosol loading. Hence, the lower feedback for higher aerosol  
loading has to be accompanied by the positive temperature dependence of the forcing. Unsurprisingly, we identify the same



dominant mechanism for these dependencies: the surface temperature dependence of emissions is masked by the aerosol, which emits largely independent of surface temperature.

375 The lower feedback for aerosol injections than for perturbations of the atmospheric CO<sub>2</sub> concentration contrasts the opposite difference simulated in GCMs (Hansen et al., 2005; Boer et al., 2006; Marvel et al., 2016; Gregory et al., 2016; Günther et al., 2022). The stronger feedback in GCM simulations with stratospheric aerosol was attributed to the differences in the surface warming patterns for aerosol and CO<sub>2</sub> forcing which are not represented in a one-dimensional column. Our interpretation is that the feedback strengthening due to the pattern effect in GCMs overcompensates the weakening from radiative causes that  
380 we find in our single column study.

The climate sensitivity is examined using surface-coupled slab ocean simulations. The temperature change in equilibrium is less temperature-dependent for the aerosol injections than for CO<sub>2</sub> forcing as the decrease in the feedback parameter is partly compensated by the decrease in forcing.

385 Even though the studied surface temperature range (280K - 300 K) is too wide for global mean surface temperatures under CO<sub>2</sub> forcing, it is not extreme in terms of regional temperature differences on Earth. Thus, the temperature dependence of the forcing and feedback might be useful to understand the impacts of volcanic eruptions or solar geoengineering at different latitudes. However, other effects such as circulation or eruption characteristics might be more important than pure radiative effects (Zanchettin et al., 2013; Aubry et al., 2022).

390 While we have studied the particular case of stratospheric sulfate aerosol, the qualitative behaviour of the forcing and feedback at different surface temperatures and the underlying reasoning should be applicable in general to any stratospheric species that weakly absorbs in the atmospheric emission window such as halocarbons (Shine and Myhre, 2020). On the other hand, this also means that the same reasoning or temperature dependence might not be applicable for other aerosols in the stratosphere that do not absorb in the atmospheric window.

395 The radiative perspective on stratospheric sulfate aerosol forcing highlights the critical role played by the longwave absorption and spectral masking by the aerosol in determining the magnitude and temperature dependence of the forcing-feedback mechanisms.

*Code and data availability.* The code and data used for the analysis and to produce the figures will be made available upon publication. konrad is available at <https://github.com/atmtools/konrad>.

400 *Author contributions.* HS and MG developed the original idea for the study and, together with RH, designed the methodology. RH performed the experiments and most of their postprocessing, and prepared the figures. CK implemented the treatment of aerosol radiative effects in konrad. RH provided the first draft of the manuscript. All authors contributed to the interpretation of the experiments and the writing of the manuscript.



<https://doi.org/10.5194/egusphere-2024-2221>

Preprint. Discussion started: 23 August 2024

© Author(s) 2024. CC BY 4.0 License.



*Competing interests.* The authors declare that they have no conflict of interest.

405 *Acknowledgements.* This work used computing resources of the Deutsches Klimarechenzentrum (DKRZ) under project ID mh0066. RH acknowledges the IISER-MPG Master Internship Program for facilitating this research. MG and CK were part of the doctoral programme of the International Max Planck Research School. CK is supported by the ETH Postdoctoral Fellowship program. The authors thank Lukas Kluff, Sally Dacie and Stefan Bühler for fruitful discussions and useful comments on an earlier version of the manuscript.. HS acknowledges funding from the Deutsche Forschungsgemeinschaft (DFG) through the projects VolARC and VolDyn of the Research Unit VolImpact (FOR2820, grant no. 398006378).



## 410 References

- Aquila, V., Oman, L. D., Stolarski, R., Douglass, A. R., and Newman, P. A.: The Response of Ozone and Nitrogen Dioxide to the Eruption of Mt. Pinatubo at Southern and Northern Midlatitudes, *Journal of the Atmospheric Sciences*, 70, 894–900, <https://doi.org/10.1175/JAS-D-12-0143.1>, publisher: American Meteorological Society Section: *Journal of the Atmospheric Sciences*, 2013.
- Aubry, T. J., Staunton-Sykes, J., Marshall, L. R., Haywood, J., Abraham, N. L., and Schmidt, A.: Climate change modulates  
415 the stratospheric volcanic sulfate aerosol lifecycle and radiative forcing from tropical eruptions, *Nature Communications*, 12, <https://doi.org/10.1038/s41467-021-24943-7>, 2021.
- Aubry, T. J., Farquharson, J. I., Rowell, C. R., Watt, S. F. L., Pinel, V., Beckett, F., Fasullo, J., Hopcroft, P. O., Pyle, D. M., Schmidt, A., and Sykes, J. S.: Impact of climate change on volcanic processes: current understanding and future challenges, *Bulletin of Volcanology*, 84, <https://doi.org/10.1007/s00445-022-01562-8>, 2022.
- 420 Bloch-Johnson, J., Rugenstein, M., Stolpe, M. B., Rohrschneider, T., Zheng, Y., and Gregory, J. M.: Climate sensitivity increases under higher CO<sub>2</sub> levels due to feedback temperature dependence, *Geophysical Research Letters*, 48, e2020GL089074, 2021.
- Boer, G. J., Stowasser, M., and Hamilton, K.: Inferring Climate Sensitivity from Volcanic Events, *Climate Dynamics*, p. 22, 2006.
- Dacie, S., Kluft, L., Schmidt, H., Stevens, B., Buehler, S. A., Nowack, P. J., Dietmüller, S., Abraham, N. L., and Birner, T.: A 1D RCE Study of Factors Affecting the Tropical Tropopause Layer and Surface Climate, *Journal of Climate*, 32, 6769 – 6782, <https://doi.org/10.1175/JCLI-D-18-0778.1>, 2019.
- 425 Fasullo, J. T., Tomas, R., Stevenson, S., Otto-Bliesner, B., Brady, E., and Wahl, E.: The amplifying influence of increased ocean stratification on a future year without a summer, *Nature Communications*, 8, <https://doi.org/10.1038/s41467-017-01302-z>, 2017.
- Forster, P., Storelvmo, T., Armour, K., Collins, W., Dufresne, J.-L., Frame, D., Lunt, D., Mauritsen, T., Palmer, M., Watanabe, M., Wild, M., and Zhang, H.: The Earth's Energy Budget, Climate Feedbacks, and Climate Sensitivity, p. 923–1054, Cambridge University Press, <https://doi.org/10.1017/9781009157896.009>, 2021.
- 430 Forster, P. M., Richardson, T., Maycock, A. C., Smith, C. J., Samset, B. H., Myhre, G., Andrews, T., Pincus, R., and Schulz, M.: Recommendations for diagnosing effective radiative forcing from climate models for CMIP6, *Journal of Geophysical Research: Atmospheres*, 121, 12,460–12,475, <https://doi.org/10.1002/2016JD025320>, 2016.
- Garcia, R. R., Randel, W. J., and Kinnison, D. E.: On the Determination of Age of Air Trends from Atmospheric Trace Species, *Journal of the Atmospheric Sciences*, 68, 139–154, <https://doi.org/10.1175/2010JAS3527.1>, publisher: American Meteorological Society Section: *Journal of the Atmospheric Sciences*, 2011.
- 435 Gregory, J. M., Ingram, W. J., Palmer, M. A., Jones, G. S., Stott, P. A., Thorpe, R. B., Lowe, J. A., Johns, T. C., and Williams, K. D.: A new method for diagnosing radiative forcing and climate sensitivity, *Geophysical Research Letters*, 31, <https://doi.org/10.1029/2003GL018747>, 2004.
- 440 Gregory, J. M., Andrews, T., Good, P., Mauritsen, T., and Forster, P. M.: Small Global-Mean Cooling Due to Volcanic Radiative Forcing, *Climate Dynamics*, 47, 3979–3991, <https://doi.org/10.1007/s00382-016-3055-1>, 2016.
- Günther, M., Schmidt, H., Timmreck, C., and Toohey, M.: Climate Feedback to Stratospheric Aerosol Forcing: The Key Role of the Pattern Effect, *Journal of Climate*, 35, 7903–7917, <https://doi.org/10.1175/jcli-d-22-0306.1>, 2022.
- 445 Hansen, J., Lacis, A., Ruedy, R., and Sato, M.: Potential climate impact of Mount Pinatubo eruption, *Geophysical Research Letters*, 19, 215–218, <https://doi.org/10.1029/91GL02788>, 1992.



- Hansen, J., Sato, M., and Ruedy, R.: Radiative forcing and climate response, *Journal of Geophysical Research: Atmospheres*, 102, 6831–6864, <https://doi.org/10.1029/96JD03436>, 1997.
- Hansen, J., Sato, M., Nazarenko, L., Ruedy, R., Lacis, A., Koch, D., Tegen, I., Hall, T., Shindell, D., Santer, B., Stone, P., Novakov, T., Thomason, L., Wang, R., Wang, Y., Jacob, D., Hollandsworth, S., Bishop, L., Logan, J., Thompson, A., Stolarski, R., Lean, J., Willson, R., Levitus, S., Antonov, J., Rayner, N., Parker, D., and Christy, J.: Climate forcings in Goddard Institute for Space Studies SI2000 simulations, *Journal of Geophysical Research: Atmospheres*, 107, ACL 2–1–ACL 2–37, <https://doi.org/10.1029/2001JD001143>, 2002.
- Hansen, J., Sato, M., Ruedy, R., Nazarenko, L., Lacis, A., Schmidt, G. A., Russell, G., Aleinov, I., Bauer, M., Bauer, S., Bell, N., Cairns, B., Canuto, V., Chandler, M., Cheng, Y., Del Genio, A., Faluvegi, G., Fleming, E., Friend, A., Hall, T., Jackman, C., Kelley, M., Kiang, N., Koch, D., Lean, J., Lerner, J., Lo, K., Menon, S., Miller, R., Minnis, P., Novakov, T., Oinas, V., Perlwitz, J., Perlwitz, J., Rind, D., Romanou, A., Shindell, D., Stone, P., Sun, S., Tausnev, N., Thresher, D., Wielicki, B., Wong, T., Yao, M., and Zhang, S.: Efficacy of climate forcings, *Journal of Geophysical Research: Atmospheres*, 110, <https://doi.org/10.1029/2005JD005776>, 2005.
- He, H., Kramer, R. J., Soden, B. J., and Jeevanjee, N.: State dependence of CO<sub>2</sub> forcing and its implications for climate sensitivity, *Science*, 382, 1051–1056, <https://doi.org/10.1126/science.abq6872>, 2023.
- Hopcroft, P. O., Kandlbauer, J., Valdes, P. J., and Sparks, R. S. J.: Reduced cooling following future volcanic eruptions, *Climate Dynamics*, 51, 1449–1463, <https://doi.org/10.1007/s00382-017-3964-7>, 2017.
- Huang, Y., Tan, X., and Xia, Y.: Inhomogeneous radiative forcing of homogeneous greenhouse gases, *Journal of Geophysical Research: Atmospheres*, 121, 2780–2789, <https://doi.org/10.1002/2015JD024569>, 2016.
- Jeevanjee, N., Seeley, J. T., Paynter, D., and Fueglistaler, S.: An Analytical Model for Spatially Varying Clear-Sky CO<sub>2</sub> Forcing, *Journal of Climate*, 34, 9463 – 9480, <https://doi.org/https://doi.org/10.1175/JCLI-D-19-0756.1>, 2021.
- Joshi, M. M. and Shine, K. P.: A GCM Study of Volcanic Eruptions as a Cause of Increased Stratospheric Water Vapor, *Journal of Climate*, 16, 3525 – 3534, [https://doi.org/10.1175/1520-0442\(2003\)016<3525:AGSOVE>2.0.CO;2](https://doi.org/10.1175/1520-0442(2003)016<3525:AGSOVE>2.0.CO;2), 2003.
- Kiehl, J. T. and Trenberth, K. E.: Earth’s Annual Global Mean Energy Budget, *Bulletin of the American Meteorological Society*, 78, 197–208, [https://doi.org/10.1175/1520-0477\(1997\)078<0197:EAGMEB>2.0.CO;2](https://doi.org/10.1175/1520-0477(1997)078<0197:EAGMEB>2.0.CO;2), publisher: American Meteorological Society Section: Bulletin of the American Meteorological Society, 1997.
- Kluft, L., Dacie, S., Buehler, S. A., Schmidt, H., and Stevens, B.: Re-Examining the First Climate Models: Climate Sensitivity of a Modern Radiative-Convective Equilibrium Model, *Journal of Climate*, 32, 8111–8125, <https://doi.org/10.1175/JCLI-D-18-0774.1>, 2019.
- Kluft, L., Dacie, S., Brath, M., Buehler, S. A., and Stevens, B.: Temperature-Dependence of the Clear-Sky Feedback in Radiative-Convective Equilibrium, *Geophysical Research Letters*, 48, <https://doi.org/10.1029/2021gl094649>, 2021.
- Koll, D. D. B. and Cronin, T. W.: Earth’s outgoing longwave radiation linear due to H<sub>2</sub>O greenhouse effect, *Proceedings of the National Academy of Sciences*, 115, 10293–10298, <https://doi.org/10.1073/pnas.1809868115>, 2018.
- Kroll, C. A., Dacie, S., Azoulay, A., Schmidt, H., and Timmreck, C.: The impact of volcanic eruptions of different magnitude on stratospheric water vapor in the tropics, *Atmospheric Chemistry and Physics*, 21, 6565–6591, <https://doi.org/10.5194/acp-21-6565-2021>, 2021.
- Kroll, C. A., Fueglistaler, S., Schmidt, H., Kornbluh, L., and Timmreck, C.: The Sensitivity of Moisture Flux Partitioning in the Cold-Point Tropopause to External Forcing, *Geophysical Research Letters*, 50, e2022GL102262, <https://doi.org/10.1029/2022GL102262>, 2023.
- Löffler, M., Brinkop, S., and Jöckel, P.: Impact of major volcanic eruptions on stratospheric water vapour, *Atmospheric Chemistry and Physics*, 16, 6547–6562, <https://doi.org/10.5194/acp-16-6547-2016>, 2016.
- Marvel, K., Schmidt, G. A., Miller, R. L., and Nazarenko, L. S.: Implications for climate sensitivity from the response to individual forcings, *Nature Climate Change*, 6, 386–389, <https://doi.org/10.1038/nclimate2888>, 2016.



- Mlawer, E. J., Taubman, S. J., Brown, P. D., Iacono, M. J., and Clough, S. A.: Radiative transfer for inhomogeneous atmospheres: RRTM, a validated correlated-k model for the longwave, *Journal of Geophysical Research: Atmospheres*, 102, 16 663–16 682, <https://doi.org/10.1029/97JD00237>, 1997.
- Pierrehumbert, R. T.: Infrared Radiation and Planetary Temperature, *AIP Conference Proceedings*, 1401, 232–244, <https://doi.org/10.1063/1.3653855>, 2011.
- Pitari, G. and Rizi, V.: An Estimate of the Chemical and Radiative Perturbation of Stratospheric Ozone Following the Eruption of Mt. Pinatubo, *Journal of the Atmospheric Sciences*, 50, 3260–3276, [https://doi.org/10.1175/1520-0469\(1993\)050<3260:AEOTCA>2.0.CO;2](https://doi.org/10.1175/1520-0469(1993)050<3260:AEOTCA>2.0.CO;2), publisher: American Meteorological Society Section: *Journal of the Atmospheric Sciences*, 1993.
- Robock, A.: Volcanic eruptions and climate, *Reviews of Geophysics*, 38, 191–219, <https://doi.org/10.1029/1998RG000054>, 2000.
- Romps, D. M.: Climate Sensitivity and the Direct Effect of Carbon Dioxide in a Limited-Area Cloud-Resolving Model, *Journal of Climate*, 33, 3413–3429, <https://doi.org/10.1175/JCLI-D-19-0682.1>, 2020.
- Rugenstein, M. A. A. and Armour, K. C.: Three Flavors of Radiative Feedbacks and Their Implications for Estimating Equilibrium Climate Sensitivity, *Geophysical Research Letters*, 48, e2021GL092 983, <https://doi.org/10.1029/2021GL092983>, 2021.
- Salvi, P., Gregory, J. M., and Ceppi, P.: Time-Evolving Radiative Feedbacks in the Historical Period, *Journal of Geophysical Research: Atmospheres*, 128, e2023JD038 984, <https://doi.org/10.1029/2023JD038984>, <https://onlinelibrary.wiley.com/doi/pdf/10.1029/2023JD038984>, 2023.
- Seeley, J. T. and Jeevanjee, N.: H<sub>2</sub>O Windows and CO<sub>2</sub> Radiator Fins: A Clear-Sky Explanation for the Peak in Equilibrium Climate Sensitivity, *Geophysical Research Letters*, 48, e2020GL089 609, <https://doi.org/10.1029/2020GL089609>, 2021.
- Shine, K. P. and Myhre, G.: The Spectral Nature of Stratospheric Temperature Adjustment and its Application to Halocarbon Radiative Forcing, *Journal of Advances in Modeling Earth Systems*, 12, e2019MS001 951, <https://doi.org/10.1029/2019MS001951>, 2020.
- Shine, K. P., Cook, J., Highwood, E. J., and Joshi, M. M.: An alternative to radiative forcing for estimating the relative importance of climate change mechanisms, *Geophysical Research Letters*, 30, <https://doi.org/10.1029/2003GL018141>, 2003.
- Simpson, S. G. C.: *Some studies in terrestrial radiation*, Edward Stanford, 1928.
- Solomon, S., Rosenlof, K. H., Portmann, R. W., Daniel, J. S., Davis, S. M., Sanford, T. J., and Plattner, G.-K.: Contributions of Stratospheric Water Vapor to Decadal Changes in the Rate of Global Warming, *Science*, 327, 1219–1223, <https://doi.org/10.1126/science.1182488>, 2010.
- Stevens, B. and Kluft, L.: A colorful look at climate sensitivity, *Atmospheric Chemistry and Physics*, 23, 14 673–14 689, <https://doi.org/10.5194/acp-23-14673-2023>, 2023.
- Toohey, M., Stevens, B., Schmidt, H., and Timmreck, C.: Easy Volcanic Aerosol (EVA v1.0): an idealized forcing generator for climate simulations, *Geoscientific Model Development*, 9, 4049–4070, <https://doi.org/10.5194/gmd-9-4049-2016>, 2016.
- Wilson, D. J. and Gea-Banacloche, J.: Simple model to estimate the contribution of atmospheric CO<sub>2</sub> to the Earth’s greenhouse effect, *American Journal of Physics*, 80, 306–315, <https://doi.org/10.1119/1.3681188>, 2012.
- Wing, A. A., Reed, K. A., Satoh, M., Stevens, B., Bony, S., and Ohno, T.: Radiative–convective equilibrium model intercomparison project, *Geoscientific Model Development*, 11, 793–813, <https://doi.org/10.5194/gmd-11-793-2018>, 2018.
- Wunderlin, E., Chiodo, G., Sukhodolov, T., Vattioni, S., Visioni, D., and Tilmes, S.: Side Effects of Sulfur-Based Geoengineering Due To Absorptivity of Sulfate Aerosols, *Geophysical Research Letters*, 51, e2023GL107 285, <https://doi.org/10.1029/2023GL107285>, <https://onlinelibrary.wiley.com/doi/pdf/10.1029/2023GL107285>, 2024.

<https://doi.org/10.5194/egusphere-2024-2221>

Preprint. Discussion started: 23 August 2024

© Author(s) 2024. CC BY 4.0 License.



Zanchettin, D., Bothe, O., Graf, H. F., Lorenz, S. J., Luterbacher, J., Timmreck, C., and Jungclaus, J. H.: Background conditions influence the decadal climate response to strong volcanic eruptions, *Journal of Geophysical Research: Atmospheres*, 118, 4090–4106, <https://doi.org/10.1002/jgrd.50229>, 2013.